Wind and Structures, *Vol. 30, No. 6 (2020) 547-558*
DOI: https://doi.org/10.12989/was.2020.30.6.547

Wind characteristics in the high-altitude difference at bridge site by wind tunnel tests

Mingjin Zhang, Jinxiang Zhang, Yongle Li, Jisheng Yu, Jingyu Zhang* and Lianhuo Wu

Department of Bridge Engineering, Southwest Jiaotong University, 610031 Chengdu, Sichuan, China

(*Received September 5, 2019, Revised January 13, 2020, Accepted March 9, 2020*)

Abstract. With the development of economy and construction technology, more and more bridges are built in complex mountainous areas. Accurate assessment of wind parameters is important in bridge construction at complex terrain. In order to investigate the wind characteristics in the high-altitude difference area, a complex mountain terrain model with the scale of 1:2000 was built. By using the method of wind tunnel tests, the study of wind characteristics including mean wind characteristics and turbulence characteristics was carried out. The results show: The wind direction is affected significant by the topography, the dominant wind direction is usually parallel to the river. Due to the sheltering effect of the mountain near the bridge, the wind speed and wind attack angle along the bridge are both uneven which is different from that at flat terrain. In addition, different from flat terrain, the wind attack angle is mostly negative. The wind profiles obey exponential law and logarithmic law. And the fitting coefficient is consistent with the code which means that it is feasible to use the method of wind tunnel test to simulate complex terrain. As for turbulence characteristics, the turbulence intensity is also related to the topography. Increases sheltering effect of mountain increases the degree of breaking up the large-scale vortices, thereby increasing the turbulence intensity. Also, the value of turbulence intensity ratio is different from the recommended values in the code. The conclusions of this study can provide basis for further wind resistance design of the bridge.

Keywords: long-span suspension bridge; high-altitude difference area; bridge site; wind characteristics; shielding effects; wind tunnel test

1. Introduction

Bridge is not only an important carrier of transportation, but also a link for economic development. The bridge can be affected by the environment. In addition to the impact of waves, earthquakes on bridge safety (Ti *et al*. 2019, 2020, Wei *et al*. 2019), wind is also a factor that should be considered in bridge design. Accurate evaluation of the wind characteristics of the bridge site area can ensure the wind-proof performance of the bridge (Xu *et al*. 2000, Bastos *et al*. 2018, Yang *et al*. 2018). With the development of economy and construction technology, more and more bridges are built in complex mountainous areas, and the study of wind characteristics in mountainous areas is gradually becoming a research hotspot. In general, numerical simulation, field measurements and wind tunnel tests are the most common research methods (Iizuka and Kondo, 2004, Rasouli *et al*. 2009, Ramechecandane and Gravdahl, 2012, Pirooz and Flay 2018, Hu *et al*. 2020).

Due to the complexity and variability of mountainous terrain, it is very difficult to explore the wind characteristics of the mountain areas. In the early period, the complex mountain was simplified into a two-dimensional and three-dimensional smooth shape to qualitatively explore the influence of terrain changes on the wind environment (Kim *et al*. 1997, Carpenter and Locke 1999, Ishihara *et al*. 1999, Salmon and Walmsley 1999).

However, the simplified methods mainly focused on the isolated hill rather than the real mountain areas. As the most direct method, field measurement is adopted by many scholars. By establishing a 50m meteorological observation tower, Hui *et al*. (2009a, 2009b) studied the wind characteristics including wind speed, wind direction, turbulence intensity, turbulence integral and spectra of the Stonecutters Bridge site in detail. In addition, a terrain modal with the scale of 1:1500 was also made and the wind characteristics under the condition of wind tunnel tests were investigated. Based on long-term monitoring data, Wang *et al*. (2009) explored the wind characteristics of the eastern coastal areas of China and the wind-induced response of long- span bridges to typhoons. The results showed that the nonstationary characteristics exist in the measured data and the wind speed calculated by the traditional method is larger than the non-stationary result. Belu and Koracin (2013) studied the spatial and temporal characteristics of the wind in complex terrain from five tall masts. Taking a long-span suspension bridge in complex terrain near the sea as the research object, the wind characteristics at the bridge site and the wind-induced vibration were investigated by setting up a series of instruments. The results showed that the wind direction in the mountainous area is obviously affected by the topography. Generally speaking, the dominant wind direction is usually consistent with the trend of the river (Fenerci and Øiseth 2017, 2018, Fenerci *et al*. 2017). By building a 50 m high meteorological mast, the wind

*Corresponding author, Ph.D. Candidate
E-mail: zhangjycd@live.com

http://www.techno-press.com/journals/was&subpage=7 ISSN: 1226-6116 (Print), 1598-6225 (Online)

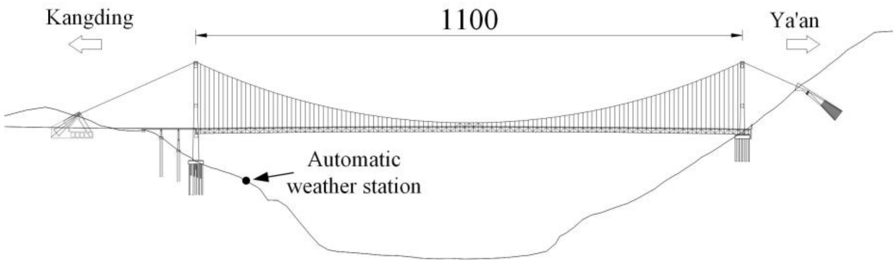

Fig. 1 Elevation of the bridge site (Unit: m)

characteristics of deep-cut canyon at different heights near the surface were investigated. The results showed that the wind characteristics at different heights near the surface are different. The attack angle is getting concentrated with the increase of anemometer, and the turbulence scale increases with the height increases while the turbulence intensity decreases (Zhang *et al*. 2020). Also taking the complex mountainous area as the research object, Huang *et al*. (2019) studied the characteristics of thunderstorm winds, and the results show that the characteristics of thunderstorm winds in complex terrain have no big difference with those in the flat area.

By combination of wind tunnel tests and numerical simulation, two terrain categories, including plain terrain and moderately rough, corresponding, respectively, to the power law exponent p=0.11 and p=0.23, were considered, and the results showed that the profiles of wind speed and turbulence intensity vary with the terrains (Mattuella *et al*. 2016). Taking a long-span bridge located in complex terrain as research object, the statistical distribution of wind field characteristics was investigated, also the insufficient of field measurement with single point mast was supplemented with wind tunnel test (Lystad *et al*. 2018). By means of experimental and numerical model, a joint method was proposed to investigate the local flow around the hill, and the spectra properties at different height above the ground level was studied as well (Ramechecandane and Gravdahl 2012, Conan *et al*. 2016, Cuerva-Tejero *et al*. 2018). Aiming at a deep-cut canyon, the shielding effect of mountain near the bridge on the wind field was conducted with numerical simulation method, and the results showed that the local terrain had significate impact on the wind field at the bridge site (Zhang *et al*. 2019). Also, the influence of thermal effect on the wind characteristics in complex terrain was investigated (Zhang *et al*. 2018). With the method of wind tunnel tests, Li *et al*. (2017) established a terrain model with the scale of 1:1000 and investigated to mean wind characteristics and pulsating wind characteristics, the results showed that the incoming wind direction has a significant effect on the wind characteristics of the bridge site area.

In the research, to study the wind characteristics at bridge site in a deep-cutting gorge, the Dadu River Bridge which straddles a deep-cutting gorge was employed as a typical example. Dadu River Bridge is also a key project of Sichuan-Tibet Expressway. The main span of the bridge is 1100m, the elevation of the main girder is 1608 m. The elevation of the bridge is shown in Fig. 1. By using wind tunnel tests, a terrain model centered on the bridge site with a diameter of 18 km was made and the scale was set as 1:2000. In order to improve the quality of the wind, a 3-D gradual curved transition sections was developed to serve as the boundary transition section of the bridge site terrain model. The effects of different oncoming wind directions on the wind characteristics over the bridge site were investigated in the simulated atmospheric boundary layer, and the wind parameters such as the mean wind speeds, power law exponents of the mean wind speed, wind attack angles, turbulence intensity, wind power spectra around the bridge were studied in detail.

2. Background of terrain model

2.1 Survey of Dadu River bridge

The topographic map of the Dadu River bridge site is shown in Fig. 2. At the bridge site, there is a prominent hill on the south side of the bridge. On the southeast side of the bridge, a ridge with an average elevation of more than 2000 m is extended. The elevation of the ridge is much higher than the design elevation of the bridge deck, so the ridge has a strong shelter effect on the bridge site area. It can be seen from Fig. 2(b) that the altitude difference within 18 km of the bridge area is large, the lowest elevation of the shape model is 1380 m, and the highest altitude is 4800 m.

Before carrying out the wind tunnel tests, an automatic weather station (AWS) was installed in the bridge site area to record the wind data. The location of the AWS can be seen from Fig. 1 and Fig. 2(a), the AWS is placed on a hillside on the Kangding side, 500m from the bridge span and 78 m below the bridge deck. The AWS is a 10 m high mast which is equipped with a 3-cup anemometer, a direction sensor and a rainfall sensor. All data is recorded by a data logger and transmitted to remote data center via cellular network. The sampling frequency of the data logger is set as 1Hz, and the output data is the average wind speed and average wind direction at ten-minute intervals. In order to ensure the reliability of the data, the built-in program will preprocess the raw data, the distortion data will be judged by 3σ principle, and the missing data and distortion data will be complete by interpolation method. Based on 3 years' data, Fig. 3 shows the corresponding rose diagram of wind direction with yearly maximum wind speed. It can be seen from the results that due to the influence of local terrain, the wind direction of the bridge site area is dominated by the south and north winds, which is consistent with the

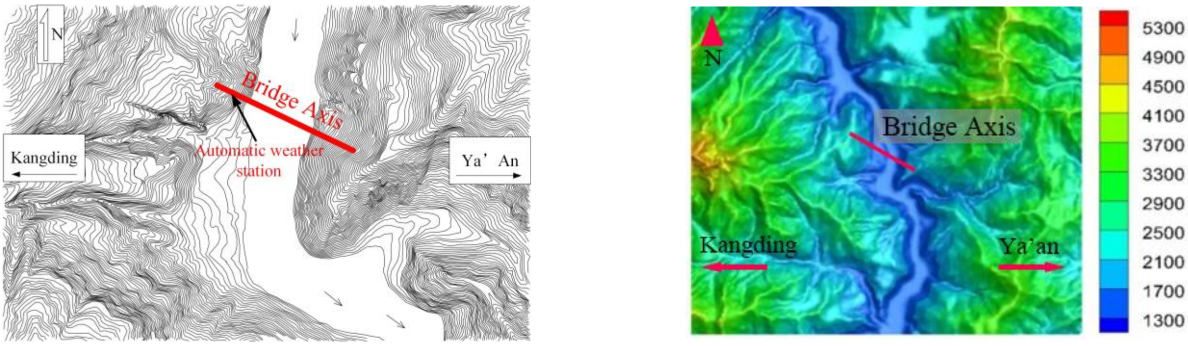

(a) Topographic map of the bridge site (b) Elevation of the bridge site (m)

Fig. 2 Terrain of the bridge site

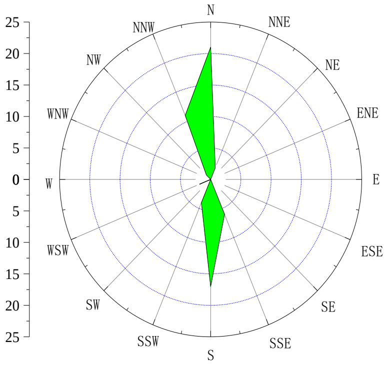

Fig. 3 Rose diagrams of wind direction with yearly maximum wind speed

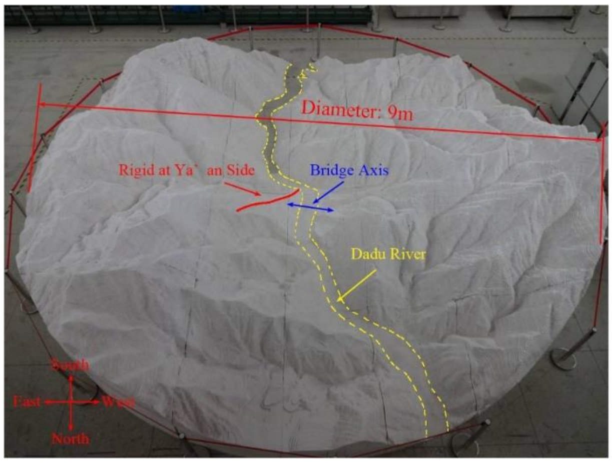

Fig. 4 Terrain model around the bridge

direction of the Dadu River at the bridge site area. The wind direction obtained by AWS is consistent with the observation results of anemometers (Yu *et al*. 2019). The wind speed at the bridge site area is also at a relatively high level. For the north wind direction, the maximum wind speed exceeds 20m/s, and for the south wind, the maximum wind speed also exceeds 15m/s. The field measured data can provide a reference for the development of subsequent wind tunnel tests. Because the wind speeds corresponding to the south and north winds are relatively large, corresponding cases should be set accordingly.

2.2 Terrain model construction around the bridge site

The wind tunnel tests were conducted in XNJD-3 wind tunnel of Southwest Jiaotong University. As one of the largest boundary layer wind tunnel in China, the test section of the wind tunnel is 22.5 m wide, 4.5 m high and 36.0 m long. To ensure the reliability of the wind characteristics in the bridge site area, the size of the terrain model should be large enough. Therefore, the scope of the terrain model was defined as a circular area with a diameter of 18 km and the scale ratio of the terrain model was set at 1/2000. At the bottom of the terrain model, the water surface of the Dadu River where the Dadu River Bridge is located is taken as the reference height. The model composed of rigid foam plate was cut and overlapped layer by layer according to terrain contour line. In the area slightly away from the bridge, the thickness of each plate is 1cm, representing the elevation difference of 20 m in full scale. The contour lines were encrypted in the core area close to the bridge site, and the plate with a layer of 0.5 cm which is corresponding to 10m in full scale was adopted to make the model. The terrain model placed in the wind tunnel is shown in Fig. 4. And the Cobra Probe was used to record the wind data. In order to improve the reliability of the tested data, all the probe used had been calibrate before test, the sampling frequency was 1000 Hz, and the sampling time was set to 3 minutes. In addition, a repeated test method (2 to 3 times) was used to verify the data.

2.3 Transition section setting

In mountainous areas, rivers are usually much lower than the surrounding mountains. Therefore, for the topographic model with the lowest elevation of water surface, the edge of the model is usually higher than that of the wind tunnel surface. Accordingly, this leads to separation or bypass of the incoming flow at the edge of the terrain model. In order to make the incoming flow transit smoothly to the model area, it is necessary to arrange reasonable airflow transition section at the boundary of the terrain model so as to make the test more accurate and reliable.

As mentioned above, the lowest altitude of the selected area is 1380 m, the highest altitude is 4800 m, and the altitude difference is 3420 m, corresponding to 1.72 m in the scaled model. In order to make the incoming flow from

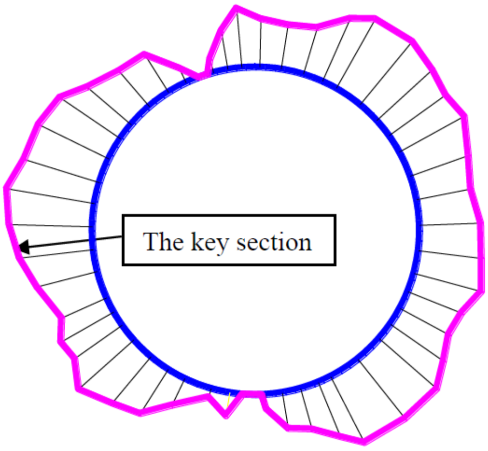

(a) The plane of transition section

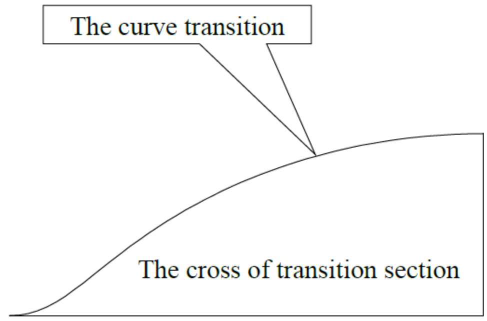

(b) The cross of transition section

(c) A part of the finished transition section

Fig. 5 Transition section for simulating terrain boundary in wind tunnel test

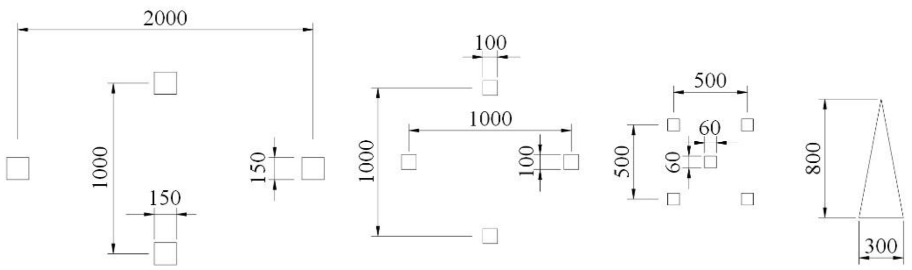

a b c d

Fig. 6 The schematic diagram of atmospheric boundary layer simulator for class D site inflow (mm): (a-c) rough element; (d) steeple

different directions can be reasonably transitioned to the bridge site, 3D curved transition sections were adopted in the test (Li *et al*. 2017). The 3D curved transition is linearly extended from the 2D curved transition which is based on the theory of cylindrical flow and potential flow (Hu *et al*. 2015). A highly linear gradient is applied to accommodate changes in the boundary topography, and the gradient slope is determined by least squares fitting based on the terrain fluctuations. In this test, according to the undulation height of the boundary of the terrain model and considering the convenience of assembling the transition section, the key sections of 47 transition sections are divided along the periphery of the terrain model. The key sections of the transition section are shown in Fig. 5(a) and Fig. 5(b). The transition section model of the typical gradient height that is produced is shown in Fig. 5(c). The blocking rate of the model in the wind tunnel is 8.8%.

3. Atmospheric boundary layer simulation

Due to the limitation of the size of the wind tunnel, the size of the terrain model is limited, so it is necessary to presuppose the inflow characteristics far from the bridge.

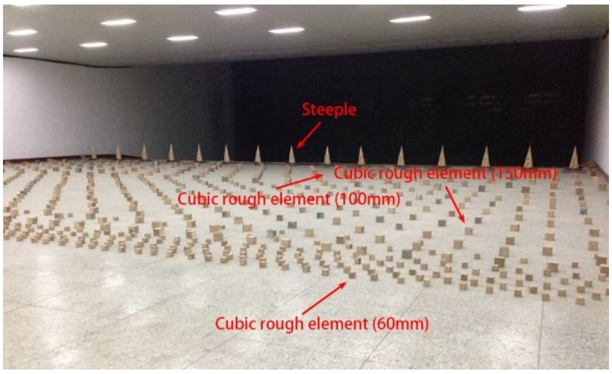

Fig. 7 Rough elements and steeples placed in wind tunnel

Fully consider the actual situation of the bridge site area and the definition of different surface types by the Chinese wind resistance code (JTG/T D60-01-2004, 2004), the atmospheric boundary layer is simulated by the D-type surface. In order to simulate the surface type, steeples and three kinds of rough elements with different sizes were used in the experiment (the specific sizes are shown in Fig. 6). The detailed arrangement is as follow: the steeple was arranged at a distance of 1.40 m from the entrance of the test section, and 15 were arranged horizontally. Rough cube elements with 150 mm edge length were arranged in 6 rows, rough cube elements with 100 mm edge length were arranged in 14 rows, and rough cube elements with 60 mm edge length were arranged in 5 rows. Rough elements and steeples arranged in the wind tunnel are shown in Fig. 7.

Before the start of the test, the wind field simulated the D-type surface which is assumed before should be calibrated. Fig. 8 is the average wind speed profile measured in the wind tunnel, and the curve fitting of the wind profile is carried out. It is shown from the graph that the wind velocity profile index fitted in the whole boundary layer height range is 0.29. Fig. 8(b) shows that the turbulence profile is in good agreement with the required value of code and theoretical values near the height of the bridge deck. The average turbulence intensity in the direction of main wind speed at the height of bridge is 17.9%. Therefore, the experimental simulation of turbulence field meets the requirements. In addition, the comparison of wind spectrum was also carried out. According to the code, the horizontal pulsating wind spectrum and the vertical pulsating wind spectrum are respectively based on the following formula:

The horizontal pulsating wind spectrum:

$$\frac{nS_u(n)}{u_*^2} = \frac{200f}{(1+50f)^{5/3}} \tag{1}$$

The vertical pulsating wind spectrum:

$$\frac{nS_w(n)}{u_*^2} = \frac{6f}{(1+4f)^2} \tag{2}$$

Where $S_u(n)$ and $S_w(n)$ are the power spectral density function in horizontal direction and vertical direction of pulsating wind respectively. n is the frequency (Hz). f is the conversion frequency, which can be obtained from

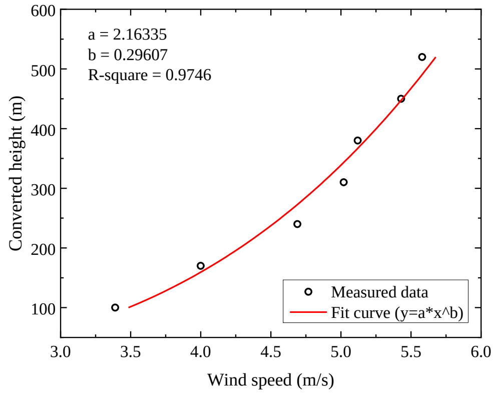

(a) Measured mean wind speed profile

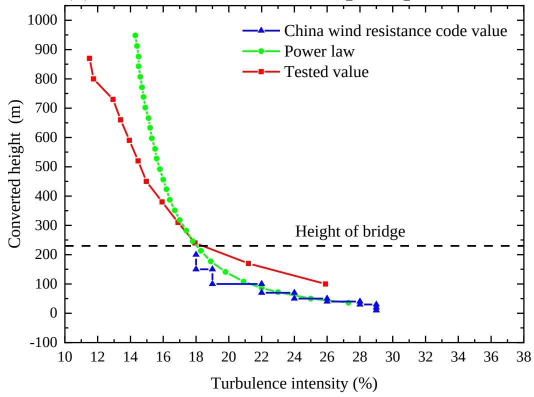

(b) Measured turbulence profile

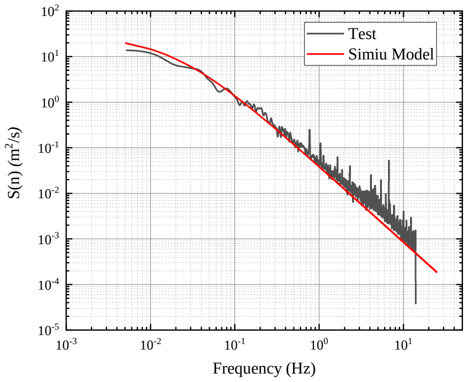

(c) Comparison of wind speed spectra between tested data and target data

Fig. 8 Comparison and verification of simulated wind field in wind tunnel test

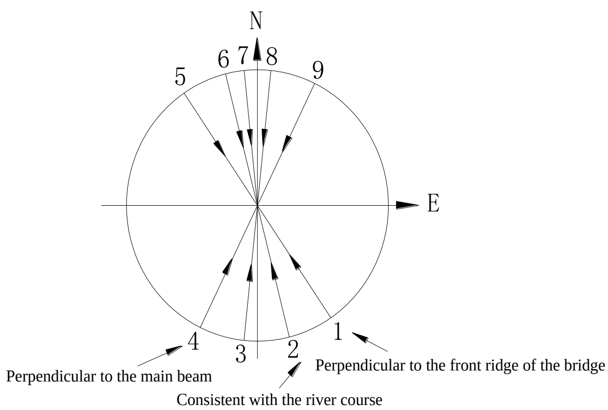

Fig. 9 Arrangement of wind directions

$f=nZ/U(Z)$, u_* is the airflow friction speed.

The comparison between simulated wind spectrum and the target wind spectrum (Simiu model) at the bridge height is shown in Fig. 8(c). It can be seen from the figure that the simulated wind spectrum is consistent with the target spectrum, which indicates that the simulated wind field can be accepted in the wind tunnel test.

4. Case configuration

The deep cut gorge where the bridge site is located is complex and changeable. Zhang *et al.* (2019) pointed that the different wind directions have great impact on the wind characteristics of the bridge site in mountainous areas. Therefore, in order to consider the effect of different directions, a total of nine wind direction were set up in the wind tunnel tests (see Fig. 9). The detailed information of each case is listed in Table 1. Case 4 and Case 9 are perpendicular to the bridge axis. The wind direction of Case 2 and Case 6 is parallel to the direction of the river. In order to investigate the sheltering effect of the ridge, two cases (Case 1 and 5) perpendicular to the ridge and three cases (Case 3, 7 and 8) are parallel to the river direction were set up. The arrangement of wind speed observation points is shown in Fig. 10. At the height of bridge deck, a total of nine data observation points was set on the main girder and the distance between adjacent observation points was 1/8 span. At mid-span, a total of 11 vertical measuring points was set up.

5. Mean wind characteristics

5.1 Mean wind speed

The wind speed profiles at mid-span are shown in Fig. 11 and Fig. 12. From the results, when the angle between wind direction and river direction is smaller and the wind direction is perpendicular to bridge axis, such as Case 1, 2, 6 and 7, the wind speed across the bridge is larger. When the wind direction is southeast wind (Case 2) and northwest wind (Case 6), the gradient wind speed ratio at the height of bridge deck is the largest, which is 0.67 and 0.52, respectively. According to the field measurement data, the dominant wind direction of the bridge site is southeast, so the further research on wind characteristics of bridge site in Case 2 should be given full attention. At the same time, it should be noted that the wind speed ratios at the height of bridge in the Case 1, 7, and 8 are relatively large. In addition, it is noted that the wind speed of the Case 1 in Fig. 12 has a tendency to increase first and then decrease with the height. This is because the Ya'an side ridge, which is perpendicular to the incoming wind in this case, has a strong sheltering effect, which leads to the difference of the wind profile at the mid-span between the bridge and the ordinary situation.

To better understand the distribution of wind speed along the bridge, Fig. 13 shows the wind speed ratio of lateral bridge at the height of main girder under north wind cases, and Fig. 14 shows the ratio of lateral bridge gradient wind speed at the height of main girder under south wind cases. It can be seen from Fig. 13 that the wind speeds of north wind cases (Case 7, 8 and 9) are generally larger at the height of bridge deck, and the gradient wind speed ratio fluctuates around 0.5. When the wind direction is northeast (Case 8 and 9), the gradient wind speed of Kangding side girder is slightly larger than that of Ya'an side. When the wind direction is northwest (Case 6 and 7), the wind speed of Ya'an side girder is larger than that of Kangding side. In case 5, due to the maximum deviation from the river, the gradient wind speed ratio at the height of bridge deck which

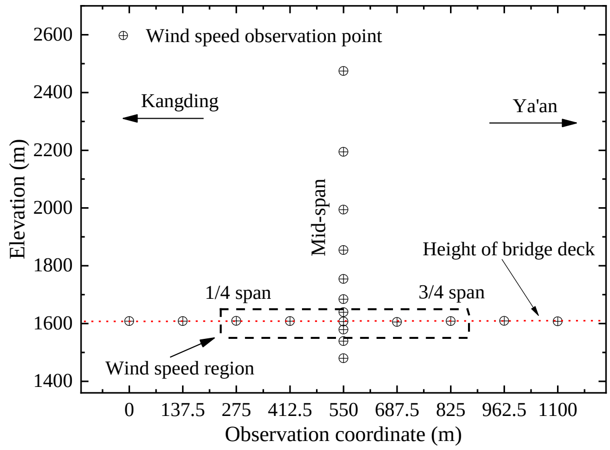

Fig. 10 Arrangement of wind speed observation points

Table 1 Arrangement of flow direction

Case no.	Direction angle (°)	Notes
1	145.9	South wind, perpendicular to the ridge in the south side
2	165.9	South wind, along the river
3	185.9	-
4	205.9	South wind, perpendicular to the bridge
5	325.9	North wind, perpendicular to the ridge in the south side
6	345.9	North wind, along the river
7	355.9	-
8	5.9	-
9	25.9	North wind, perpendicular to the bridge

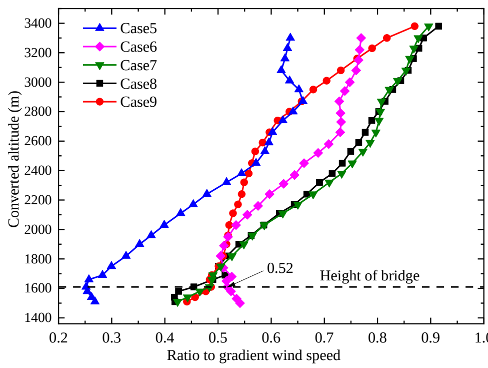

Fig. 11 The wind speed profile at mid-span in the north wind

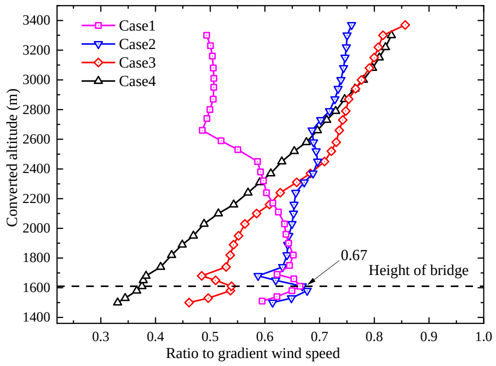

Fig. 12 The wind speed profile at mid-span in the south wind

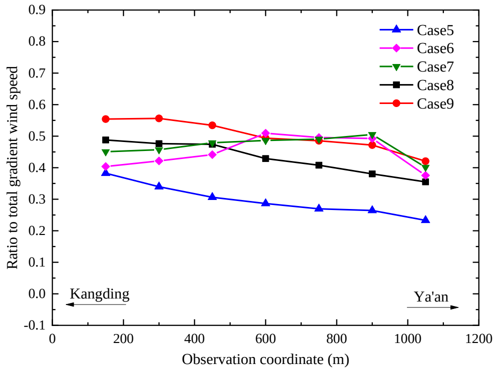

Fig. 13 The lateral wind speed ratio at the height of bridge deck under north wind cases

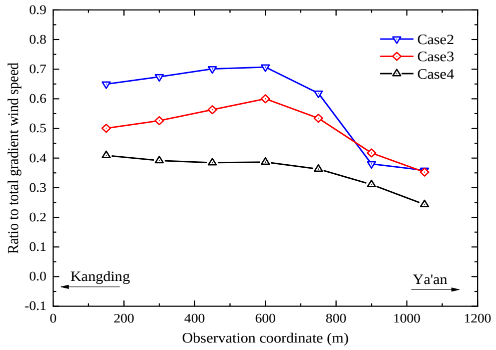

Fig. 14 The lateral wind speed ratio at the height of bridge deck under south wind cases

is less than 0.4. Generally speaking, under the north wind cases, the wind speed along the bridge is relatively uniform at the height of bridge deck, and there is no obvious sudden change, but the wind speed is larger. In addition, the same phenomenon can be found in the field measurement at the same place. From the observation results of field measurement, both mean wind speed and the maximum speed decrease from Kangding side to Ya;an side (Yu *et al.* 2019). As it can be seen from Fig. 14, due to the sheltering effect of Ya'an side ridge, the wind speed distribution along the bridge is severely uneven, and the wind speed of Kangding side is obviously accelerated. The wind speed is generally lower at Ya'an side. In Case 2, the minimum gradient wind speed ratio is 0.35, while the maximum

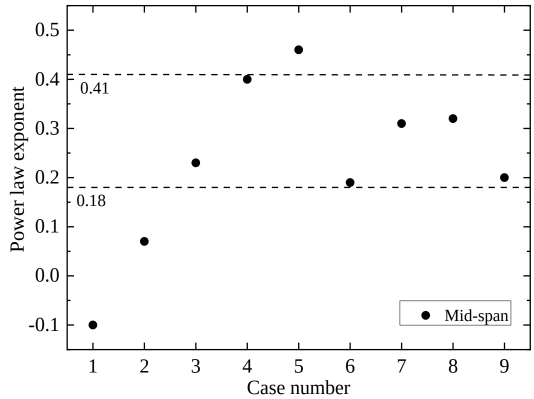

Fig. 15 Fitting coefficient of wind profile at midspan of main girder

gradient wind speed ratio at Kangding side is 0.71. Therefore, the bridge response caused by non-uniform load should be paid enough attention, especially southeast wind, which often produces larger wind speed in winter.

5.2 Wind profile exponent

The exponential law fitting of the lateral wind speed at mid-span with different wind directions is carried out. The fitting results are shown in Fig. 15. It can be seen from the figure that the wind profile exponent fitted under different cases is discrete and significantly different, and even have negative values. The difference in wind profile exponent qualitatively illustrates the wind characteristics at mid-span affect by wind direction and topography. When the wind direction is perpendicular to the axes of the bridge and there is no mountain shelter in front of the bridge (such as Case 7, 8 and 9) The fitting results are relatively stable and generally conform to the exponential law. The average value of the wind profile exponent and the required value of the code is 0.28 and 0.3 respectively.

5.3 Wind attack angle

For most bridges in flat areas, the wind angle range is between -3 and +3°, but for the Dadu River bridge located in complex mountainous terrain, the wind attack angle in the bridge area may be larger 21,26. Under different cases, the change of wind attack angle with height at mid-span is shown in Fig. 16 and Fig. 17. From Case 5 to Case 9, the wind attack angle of the mid-span is small, all of which are between -2° and +2°. Due to the sheltering effects of mountains in front of the bridge, the disturbed flow makes the wind attack angle under south wind cases larger generally, and most of them are negative wind attack angle. The maximum wind attack angle at the height of bridge reaches -10.3°, which is larger than the given value of the code. The distribution law of the wind attack angle is also consistent with the measured results (Zhang *et al.* 2015; Zhang, 2016). Based on the field measurement, the wind angle of attack at the design height of the bridge deck is mainly negative, and the average wind angle of attack is -4.5° which is larger than that in flat area.

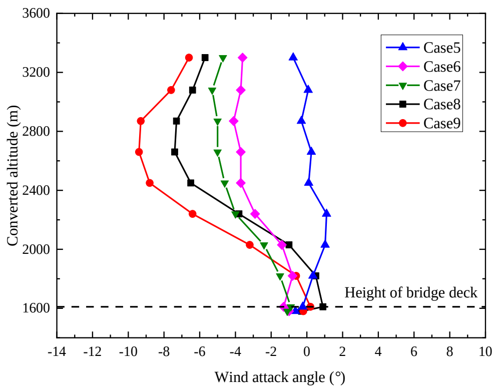

Fig. 16 Variation of attack angle with height at midspan under north wind cases

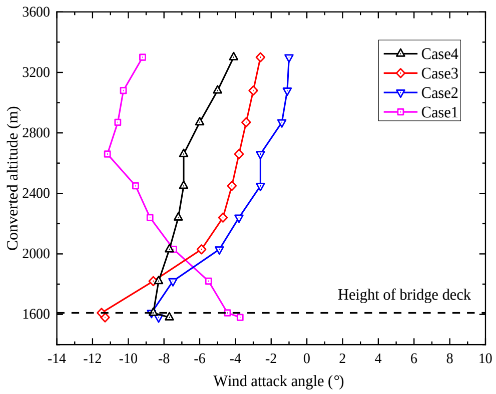

Fig. 17 Variation of attack angle with height at midspan under south wind cases

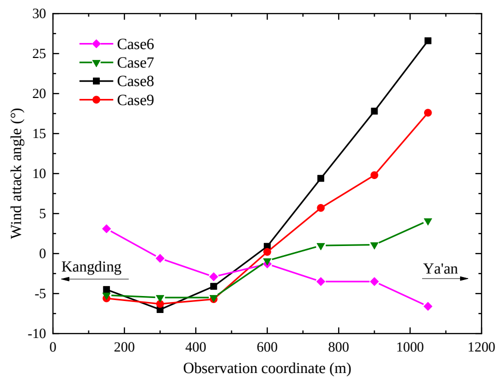

Fig. 18 Variation of wind attack angles along the bridge at different positions under north wind cases

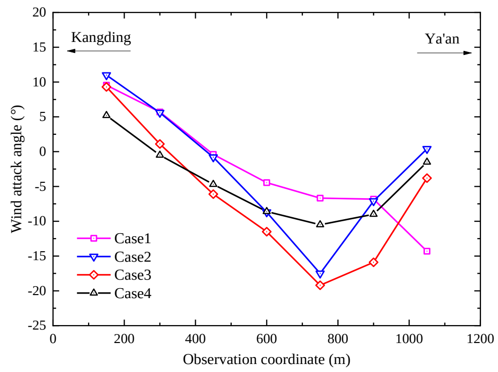

Fig. 19 Variation of wind attack angles along the bridge at different positions under south wind cases

To study the variation of wind attack angle along the bridge, the variation of the wind attack angle at the height of bridge deck under north and south wind cases is shown in Fig. 18 and Fig. 19, respectively. As can be seen from Fig. 18, under north wind cases, the wind attack angle at Kangding side is mainly negative while that at Ya'an side is positive. It can be explained as follow: For the north wind cases, the wind direction from Ya'an side is slightly higher than the ridge of the bridge deck, when the Oncoming stream crosses the ridge and reaches the bridge deck, the wind is subducted downward, so the wind attack angle of Kangding side is negative.

On the Ya'an side, due to the sheltering effect of high ridge behind the bridge, when the wind encounters the ridge, it will rise upward, which will make the main girder at Ya'an side have a larger positive wind attack angle. From Fig. 19, it can be found that the wind attack angle under south wind cases is opposite to that of the north wind. The reason should be consistent with north wind cases. Thus, under south wind cases. A slight sheltering effect of the ridge at Kangding side will rise the airflow, which makes the wind attack angle at Kangding side positive. For the Ya'an side, the wind over the ridge will subduct downward, which makes the wind attack angle at Ya'an side negative. Although the wind attack angle is larger at a certain point along the bridge, the average wind attack angle is not large. Also, the same change law of wind attack angle along the bridge axis can be found in the numerical model and field measurement (Zhang 2016, Zhang *et al*. 2019).

5.4 Interaction among wind speed, wind direction and wind attack angle

The variation of wind direction and wind attack angle at the height of bridge deck is shown in Fig. 20. The results show that the wind direction has great influence on wind speed and wind attack angle, and wind speed generally decreases with the increase of wind attack angle. Also, there is a good consistency between wind speed and wind attack angle. For all test cases, the wind attack angle is mainly negative under south wind cases. When the wind direction is parallel to the river, the wind speed is larger and the wind attack angle is relatively small. When the angle between wind direction and river is large, the wind attack angle increases gradually and even reach about -10° in some cases. However, the larger wind attack angle corresponds to relatively small wind speed and negative attack angle, so these cases cannot control the wind resistance of the structure.

The relationship of wind speed and wind attack angle at midspan of the main girder is shown in Fig. 21. It can be seen from the figure that the high wind speed is mainly concentrated in the area where the wind attack angle is around -5°. In order to facilitate the follow-up bridge model test and wind-induced response analysis, the solid line in the Fig. 21 is used to represent the corresponding relationship between wind speed and wind attack angle.

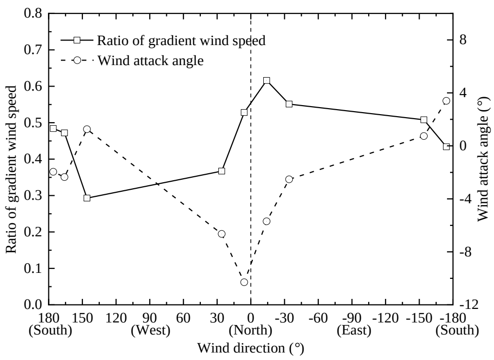

Fig. 20 Variation of wind speed and wind attack angle at mid-span with wind direction

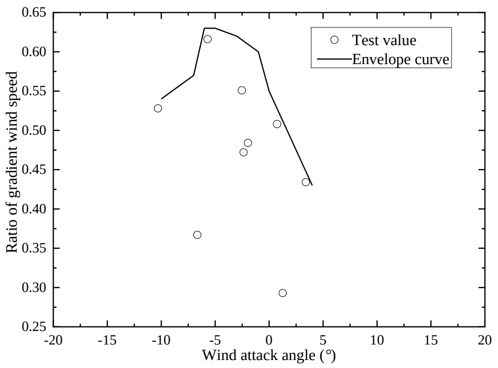

Fig. 21 Variation of wind speed with wind attack angle

From the figure, it can be seen that the solid line well envelops the calculation results of various cases.

6. Turbulence characteristic at bridge site

6.1 Turbulence intensity

The turbulence intensity under different cases are shown in Table 2. From the results, the turbulent intensity with less shielding in the north wind cases (Cases 6 - 9) is relatively small, the turbulence intensity in along wind direction corresponding to Cases 6 to 9 is 18.8%, 21.3%, 17.5% and 15.8%. While the turbulence intensity increases significantly for Cases 4 & 5 with severe shielding. This is mainly due to the fact that the wind directions in Cases 6 - 9 is generally parallel to the river, the terrain is relatively flat and the degree of airflow separation is not large. For the cases which angle between wind direction and the river is relatively large, the turbulence intensifies gradually increase due to the effect of terrain, and the separation degree of airflow increases with the obstruction of terrain. In addition, the turbulence intensity ratio I_v/I_u and I_w/I_u at the height of bridge deck is also given in the table. It can be seen from the table that the value of turbulence intensity ratio is different from the recommended values in the code where $I_v/I_u$is 0.88 and I_w/I_u is 0.5. Also, the turbulence intensity ratio obtained from field measurement has the same property (Yu *et al*. 2019, Zhang *et al*. 2020). This phenomenon indicates that the bridges located in mountainous areas cannot be designed in full accordance with the code, but must be designed according to the characteristics of the location of the bridge site. The difference further shows that the pulsating wind characteristics of the mountain gorge terrain are different from that of flat terrain.

Table 2 Turbulence intensity values at bridge deck height under different cases (%)

Case no.	I_u	I_v	I_w	I_u: I_v	I_u: I_w
1	15.5	13	11.7	1:0.76	1:0.84
2	12.6	8.5	7.95	1:0.63	1:0.68
3	14	13.9	11.5	1:0.82	1:0.99
4	26.7	23.5	21.6	1:0.81	1:0.88
5	36.2	29.2	24.3	1:0.67	1:0.81
6	18.8	16.8	13.5	1:0.72	1:0.89
7	21.3	16.8	13.4	1:0.63	1:0.79
8	17.5	19.9	15.3	1:0.87	1:1.14
9	15.8	18.9	12.4	1:0.79	1:1.20

6.2 wind power spectra

The longitudinal wind spectra model adopted by bridge wind engineering in China is Simiu spectra, but it should be noted that the Simiu spectra is based on wind speed data in flat areas. For mountain canyon terrain, topographic fluctuations may lead to the changes in energy distribution of wind spectrum. The comparison of the measured wind spectra at midspan and the Simiu spectra is shown in Fig. 22. From the results, when the wind direction is parallel to the river, the measured wind spectra of the mid-span is closer to Simiu model. With the increase of the angle between wind direction and river, the wind spectrum in the span of main girder moves more obviously to the high frequency direction than that in Simiu model. This is because the energy values at different frequencies of the wind vary significantly depending on the terrain. Therefore, under the conditions that the angle between wind direction and river is larger or the wind is blocked by the mountain, the vortex scale of the airflow is reduced significantly, and the energy of the high-frequency component in the wind spectrum is increased more obviously. In order to show the difference between these spectra, the fitted curve of each spectra is also shown in Fig. 22. According to the Simiu model, the wind spectrum is assumed as follow:

$$\frac{nS(n)}{u_*^2} = \frac{Af}{(1+Bf)^{5/3}} \tag{3}$$

Where A and B are the coefficients need to be fit.

From the results, the values of A and B are affected by the local terrain and the wind direction of incoming flow. When the wind direction is consistent with the river direction or is perpendicular to the bridge axis, the values of A and B in south wind cases are greater than that in the north wind cases. When the wind direction is perpendicular to the protruding ridge on the south side of the bridge, the values of A and B in north wind cases are greater than that in the south wind cases.

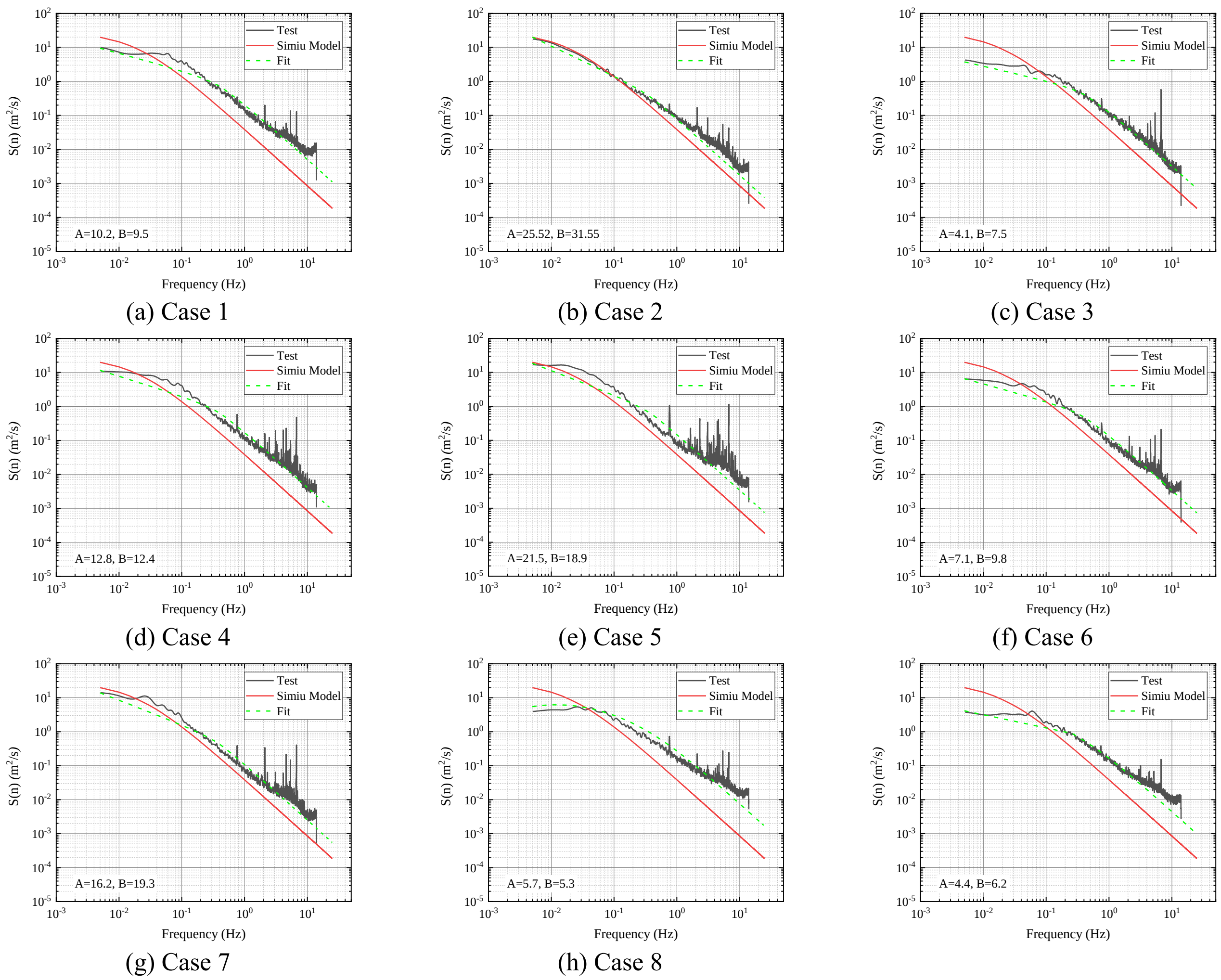

(a) Case 1 (b) Case 2 (c) Case 3

(d) Case 4 (e) Case 5 (f) Case 6

(g) Case 7 (h) Case 8

Fig. 22 Comparison between the wind power spectra at the mid-span point obtained from the wind tunnel test and the Simiu model

7. Conclusions

In this paper, a wind tunnel test method is used to establish the complex mountainous terrain model with the range of 18km in the scale of 1:2000, and the wind characteristics of the deep canyon bridge site are discussed. Through research, the following conclusions can be drawn:

The change of wind direction in the bridge site is very complex, which will be affected by the incoming wind direction and local topography. In addition, due to the influence of terrain, the distribution of wind speed along the bridge axis is different under different incoming wind direction. The unbalanced wind speed distribution along the bridge will make the wind load distribution along the bridge deviate greatly, which should be paid attention to in the wind resistance design of the bridge and in the further study.

For the bridge located in the complex mountainous area, the negative wind attack angle is majority, and the wind attack angle has a strong correlation with the incoming wind direction. Through the wind tunnel tests, the maximum wind angle of attack is $-10.3°$, which is much higher than that in the plain or coastal areas. In the follow-up study, we should pay attention to it. In addition, similar to the distribution of wind speed, the distribution of wind attack angle along the bridge axis is also uneven, and the direction of the dominant wind attack angle at different positions of the bridge may even be reversed. When the wind profile at midspan is fitted by exponential function, the mean value of the fitted values is 0.28, which is consistent with the surface roughness coefficient 0.30.

For the cases which wind direction is perpendicular to the bridge axis, the turbulence intensity is relatively small. However, with the angle between the wind and the river increases, the turbulence intensity increases obviously. In addition, the emergence of the protruding mountain in front of the bridge will also increase the turbulence intensity. Also, the turbulence ratios I_v/I_u and I_w/I_u are different from that in flat terrain.

Through this study, it can be found that it is not enough to determine the wind characteristics of the bridge site by wind tunnel tests. Therefore, wind tunnel experiments, numerical simulations, and field measurements are essential. The three have their own advantages and disadvantages. The wind tunnel experiment has a low Reynolds number and a limited model size. The accuracy of numerical simulation on the analysis of wind characteristics in complex mountain areas needs to be improved. Therefore, the wind characteristics in such areas need to be determined comprehensively by various methods.

Acknowledgments

The work described in this paper was fully supported by a grant from the National Key Research and Development Program of China (No. 2018YFC1507800), grants from the National Natural Science Foundation of China (nos. 51525804, 51708464), a grant from Primary Research & Development Plan of Sichuan Province (2019YFG0001), a grant from the Hunan Provincial Transportation Science and Technology Project (No. 201615), and a grant from the Fundamental Research Funds for the Central Universities (No. 2682019CX02).

References

Bastos F., Caetano E., Cunha Á., Cespedes X. and Flamand O. (2018), "Characterisation of the wind properties in the Grande Ravine viaduct", *J. Wind Eng. Ind. Aerod*., **173**, 112-131. https://doi.org/10.1016/j.jweia.2017.12.0https://doi.org/10.1016/j.jweia.2017.12.012 12.

Belu R. and Koracin D. (2013), "Statistical and spectral analysis of wind characteristics relevant to wind energy assessment using tower measurements in complex terrain", *J. Wind Energy*, 2013, 1-12. https://doi.org/10.1155/2013/739162.

Carpenter P. and Locke N. (1999), "Investigation of wind speeds over multiple two-dimensional hills", *J. Wind Eng. Ind. Aerod*., **83**(1), 109-120. https://doi.org/10.1016/S0167-6105(99)00065-3.

Conan, B., Chaudhari, A., Aubrun, S., Van Beeck, J., Hämäläinen, J. and Hellsten, A. (2016), "Experimental and numerical modelling of flow over complex terrain: The bolund hill", *Bound. Layer Meteorol*., **158**(2), 183-208. https://doi.org/10.1007/s10546-015-0082-0.

Cuerva-Tejero A., Avila-Sánchez S., Gallego-Castillo C., López-García Ó., Pérez-Alvarez J. and Yeow T.S. (2018), "Measurement of spectra over the Bolund hill in wind tunnel", *Wind Energy*, **21**(2), 87-99. https://doi.org/10.1002/we.2146.

Fenerci A. and Øiseth O. (2017), "Measured buffeting response of a long-span suspension bridge compared with numerical predictions based on design wind spectra", *J. Struct. Eng*., **143**(9), 04017131. https://doi.org/10.1061/(ASCE)ST.1943-541X.0001873.

Fenerci A. and Øiseth O. (2018), "Strong wind characteristics and dynamic response of a long-span suspension bridge during a storm", *J. Wind Eng. Ind. Aerod*., **172**, 116-138. https://doi.org/10.1016/j.jweia.2017.10.030.

Fenerci A., Øiseth O. and Rønnquist A. (2017), "Long-term monitoring of wind field characteristics and dynamic response of a long-span suspension bridge in complex terrain", *Eng. Struct*., **147**(15), 269-284. https://doi.org/10.1016/j.engstruct.2017.05.070.

Hu, P., Han, Y., Xu, G., Cai, C.S. and Cheng, W. (2020), "Effects of inhomogeneous wind fields on the aerostatic stability of a long-span cable-stayed bridge located in a mountain-gorge terrain", *J. Aerosp. Eng*., **33**(3), https://doi.org/10.1061/(ASCE)AS.1943-5525.0001117.

Hu, P., Li, Y.L., Huang, G.Q., Kang, R. and Liao, H.L. (2015), "The appropriate shape of the boundary transition section for a mountain-gorge terrain model in a wind tunnel test", *Wind Struct*., **20**(1), 15-36. http://dx.doi.org/10.12989/was.2015.20.1.015.

Huang, G., Jiang, Y., Peng, L., Solari, G., Liao, H. and Li, M. (2019), "Characteristics of intense winds in mountain area based on field measurement: Focusing on thunderstorm winds", *J. Wind Eng. Ind. Aerod*., **190**, 166-182. https://doi.org/10.1016/j.jweia.2019.04.020.

Hui M.C.H., Larsen A. and Xiang H.F. (2009a), "Wind turbulence characteristics study at the Stonecutters Bridge site: Part II: Wind power spectra, integral length scales and coherences", *J. Wind Eng. Ind. Aerod*., **97**(1), 48-59. https://doi.org/10.1016/j.jweia.2008.11.003.

Hui M.C.H., Larsen A. and Xiang H.F. (2009b), "Wind turbulence characteristics study at the Stonecutters Bridge site: Part I—Mean wind and turbulence intensities", *J. Wind Eng. Ind. Aerod*., **97**(1), 22-36. https://doi.org/10.1016/j.jweia.2008.11.002.

Iizuka, S. and Kondo, H. (2004), "Performance of various sub-grid scale models in large-eddy simulations of turbulent flow over complex terrain", *Atmos. Environ*., **38**(40), 7083-7091. https://doi.org/10.1016/j.atmosenv.2003.12.050.

Ishihara, T., Hibi, K. and Oikawa, S. (1999), "A wind tunnel study of turbulent flow over a three-dimensional steep hill", *J. Wind Eng. Ind. Aerod*., **83**(1-3), https://doi.org/10.1016/S0167-6105(99)00064-1.

JTG/T D60-01-2004 (2004), "Wind-resistent design specification for highway bridges ministry of transport of the people's Republic of China, Beijing", China (in Chinese).

Kim, H.G., Lee, C.M., Lim, H.C. and Kyong, N.H. (1997), "An experimental and numerical study on the flow over two-dimensional hills", *J. Wind Eng. Ind. Aerod*., **66**(1), 17-33. https://doi.org/10.1016/S0167-6105(97)00007-X.

Li Y., Hu P., Xu X., and Qiu J., (2017), "Wind characteristics at bridge site in a deep-cutting gorge by wind tunnel test", J. Wind Eng. Ind. Aerodyn., 160, 30–46.

Lystad, T.M., Fenerci, A. and Øiseth, O. (2018), "Evaluation of mast measurements and wind tunnel terrain models to describe spatially variable wind field characteristics for long-span bridge design", *J. Wind Eng. Ind. Aerod*., **179**, 558-573. https://doi.org/10.1016/j.jweia.2018.06.021.

Mattuella, J.M.L., Loredo-Souza, A.M., Oliveira, M.G.K., and Petry, A.P. (2016), "Wind tunnel experimental analysis of a complex terrain micrositing", *Renew. Sustain. Energy Rev*., **54**, 110-119. https://doi.org/10.1016/j.rser.2015.09.088.

Mingjin, Z., Jisheng, Y., Jingyu, Z., Lianhuo, W. and Yongle, L. (2019), "Study on the wind-field characteristics over a bridge site due to the shielding effects of mountains in a deep gorge via numerical simulation", *Adv. Struct. Eng*., **22**(14), 3055-3065. https://doi.org/10.1177%2F1369433219857859.

Pirooz, A.A.S. and Flay, R.G.J. (2018), "Comparison of speed-up over hills derived from wind-tunnel experiments, wind-loading standards and numerical modelling", *Bound. Layer Meteorol*., **168**(2), 213-246. https://doi.org/10.1007/s10546-018-0350-x.

Ramechecandane, S. and Gravdahl, A.R. (2012), "Numerical investigations on wind flow over complex terrain", *Wind Eng*., **36**(3), 273-295. https://doi.org/10.1260%2F0309-524X.36.3.273.

Rasouli A., Hangan H., and Siddiqui K., (2009), "PIV measurements for a complex topographic terrain", J. Wind Eng. Ind. Aerodyn., 97(5), 242–254.

Salmon, J.R. and Walmsley, J.L. (1999), "A two-site correlation model for wind speed, direction and energy estimates", *J. Wind Eng. Ind. Aerod*., **79**(3), 233-268. https://doi.org/10.1016/S0167-6105(98)00119-6.

Ti, Z., Wei, K., Li, Y. and Xu, B. (2020), "Effect of wave spectral variability on stochastic response of a long-span bridge subjected to random waves during tropical cyclones", *J. Bridge Eng*., **25**(1), https://doi.org/10.1061/(ASCE)BE.1943-

5592.0001517.
Ti, Z., Zhang, M., Li, Y. and Wei, K. (2019), "Numerical study on the stochastic response of a long-span sea-crossing bridge subjected to extreme nonlinear wave loads", *Eng. Struct.*, **196**(1), https://doi.org/10.1016/j.engstruct.2019.109287.
Wang, H., Li, A., Guo, T. and Xie, J. (2009), "Field measurement on wind characteristic and buffeting response of the Runyang Suspension Bridge during typhoon Matsa", *Sci. China Ser. E Technol. Sci.*, **52**(5), 1354-1362. https://doi.org/10.1007/s11431-008-0238-y.
Wei, K., Zhang, J. and Qin, S. (2019), "Experimental and numerical assessment into frequency domain dynamic response of deep water rigid-frame bridge", *J. Earthq. Eng.*, 1-24. https://doi.org/10.1080/13632469.2019.1684402.
Xu, Y.L., Zhu, L.D., Wong, K.Y. and Chan, K.W.Y. (2000), "Field measurement results of Tsing Ma suspension Bridge during Typhoon Victor", *Struct. Eng. Mech.*, **10**(6), 545-559. https://doi.org/10.12989/sem.2000.10.6.545.
Yang, D.H., Yi, T.H., Li, H.N. and Zhang, Y.F. (2018), "Monitoring-based analysis of the static and dynamic characteristic of wind actions for long-span cable-stayed bridge", *J. Civ. Struct. Health Monit.*, **8**(1), 5-15. https://doi.org/10.1007/s13349-017-0257-0.
Yu, C., Li, Y., Zhang, M., Zhang, Y. and Zhai, G. (2019), "Wind characteristics along a bridge catwalk in a deep-cutting gorge from field measurements", *J. Wind Eng. Ind. Aerod.*, 186, 94-104. https://doi.org/10.1016/j.jweia.2018.12.022.
Zhang M. (2016), "Field measurement and numerical simulation of wind characteristics of bridge site in complex terrain", Ph. D. Dissertation, Southwest Jiaotong University, China.
Zhang, J., Zhang, M., Li, Y. and Fang, C. (2020), "Comparison of wind characteristics at different heights of deep-cut canyon based on field measurement", *Adv. Struct. Eng.*, **23**(2), 219-233. https://doi.org/10.1177%2F1369433219868074.
Zhang, M., Li, Y., Tang, H., Zhu, L. and Tao, Q. (2015), "Field measurement of wind characteristics at bridge site in deep gorge with high altitude and high temperature difference", *China J. Highw. Transp.*, **28**(3), 60-65.
Zhang, M., Li, Y., Wang, B. and Ren, S. (2018), "Numerical simulation of wind characteristics at bridge site considering thermal effects", *Adv. Struct. Eng.*, **21**(9), 1313-1326. https://doi.org/10.1177%2F1369433217742524.

FR